NUMERICAL STUDIES OF OPEN CHANNEL FLOWS AROUND INCLINED SPUR DIKES BY MEANS OF A NON-LINEAR k-ε MODEL

Ichiro Kimura
Faculty of Environmental and Information Sciences, Yokkaichi University
1200 Kayo-cho, Yokkaichi 512-8512, Japan
kimura@yokkaichi-u.ac.jp

Takashi Hosoda
Department of Civil Engineering, Kyoto University
Yoshida Sakyo-ku, Kyoto 606-8501, Japan
hosoda@riv.kuciv.kyoto-u.ac.jp

Shinichiro Onda
Graduate School of Civil Engineering, Kyoto University
Yoshida Sakyo-ku, Kyoto 606-8501, Japan
sonda@riv.kuciv.kyoto-u.ac.jp

Akihiro Tominaga
Department of Architecture and Civil Engineering, Nagoya Institute of Technology
Gokiso-cho Showa-ku, Nagoya 466-8555, Japan
tomi@suiko1.ace.nitech.ac.jp

ABSTRACT

Characteristics of 3D turbulent flow features around inclined submerged spur dikes are numerically investigated using a non-linear k-ε model. A generalized curvilinear movable coordinate is employed to calculate the free surface oscillation and take into account the complex topography. The computations were performed under the conditions of the laboratory tests with PIV measurements performed by Tominaga et al (2001). Numerical results show that the amplitude of fluid oscillation around downstream inclined spur dikes is much larger than that around downstream inclined ones and the period of the oscillation is in compatible with the first mode of impinging shear layer.

INTRODUCTION

Spur dikes have been constructed in rivers to protect riverbanks from erosion and maintain the routes for navigation. Recently, the main role of the spur dikes is changing, that is, spur dikes become to be focused as structures for environmental functions. The sedimentation around a submerged spur dike is closely affected by its inclination angle. Therefore, it is important to clarify the effects of the inclination angle on 3D flow structures around the spur dikes.

In this study, characteristics of 3D turbulent flows around the submerged spur dikes are numerically investigated using a non-linear k-ε model. A generalized curvilinear movable coordinate is employed to simulate the free surface oscillation and take into account the complex topography. The computations were performed under the conditions of the laboratory tests with PIV measurements performed by Tominaga et al (2001). The time-averaged and time-dependent flow features are discussed through the comparison between the computational and experimental results.

COMPUTATIONAL MODEL

Basic Equations

Basic equations with contravariant components of velocity vectors on a generalized curvilinear movable coordinate system are described as follows.

[Continuity equation]

$$\frac{1}{\sqrt{g}}\frac{\partial V^{\alpha}\sqrt{g}}{\partial \xi^{\alpha}} = 0 \tag{1}$$

[Momentum equation]

$$\frac{\partial V^{i}}{\partial t} + \nabla_j\left[V^{j}(V^{j} - W^{j})\right] + V^{j}\nabla_j W^{j} + V^{j}\nabla_j W^{i} = F^{i} - \frac{1}{\rho}g^{ij}\nabla_j p + \nabla_j\left[-\overline{v^{i}v^{j}}\right] + 2\nu\nabla_j e^{ij} \tag{2}$$

[k-ε equations]

$$\frac{\partial k}{\partial t} + \nabla_j\left[k(V^{j} - W^{j})\right] + k\nabla_j W^{j} = -g_{il}\overline{v^{l}v^{j}}\nabla_j V^{i} - \varepsilon + \nabla_j\left\{\left(\frac{D_t}{\sigma_k} + \nu\right)g^{ij}\nabla_i k\right\} \tag{3}$$

$$\frac{\partial \varepsilon}{\partial t} + \nabla_j\left[\varepsilon(V^{j} - W^{j})\right] + \varepsilon\nabla_j W^{j} = -C_{\varepsilon 1}\frac{\varepsilon}{k}g_{il}\overline{v^{l}v^{j}}\nabla_j V^{i} - C_{\varepsilon 2}\frac{\varepsilon^{2}}{k} + \nabla_j\left\{\left(\frac{D_t}{\sigma_k} + \nu\right)g^{ij}\nabla_i \varepsilon\right\} \tag{4}$$

Table 1: Hydraulic conditions in the flow field.

Channel width	0.3 m,	Bed slope	1/2000
Averaged depth	8.0 cm,	Discharge	4.1 l/s
Averaged velocity	17.1 cm/s,	Froude number	0.193
Reynolds number	13660,	Length of spur dikes	5.0 cm
Width of spur dikes	2.0 cm,	Height of spur dikes	4.0 cm

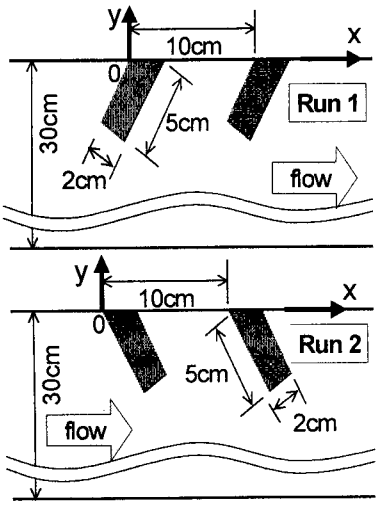

Figure 1: Flow field and coordinate in the computation.

where ξ^i = generalized curvilinear coordinate, t = time, V^i = contravariant component of the velocity vector of flows, W^i = contravariant component of the velocity vector of grid motion, p = pressure, ν= molecular dynamic viscosity, ρ = density of water, k = turbulent energy, ε = turbulent energy dissipation rate, g_{ij} and g^{ij} = covariant and contravatiant component of metric tensor, g = det(g_{ij}) and F^i = contravariant component of gravity acceleration. ∇^i indicates a covariant differential, for instance,

$$\nabla_i A^k = \frac{\partial A^k}{\partial \xi^i} + A^j \Gamma_{ij}^{\ k} \tag{5}$$

where $\Gamma_{ij}^{\ k}$ = Christoffel symbol described as

$$\Gamma_{ij}^{\ k} = \left\{ \begin{matrix} k \\ i\,j \end{matrix} \right\} = \frac{1}{2} g^{km} \left(\frac{\partial g_{jm}}{\partial \xi^i} + \frac{\partial g_{im}}{\partial \xi^j} - \frac{\partial g_{ij}}{\partial \xi^m} \right) = \frac{\partial \xi^k}{\partial x^p} \frac{\partial^2 x^p}{\partial \xi^i \partial \xi^j} \tag{6}$$

Turbulence Model

To calculate a complex turbulent flow with separation and vortex shedding, a 2nd-order non-linear k-ε model by Kimura and Hosoda (2000) is adopted as a turbulence model. This model has been applied to various flow fields with the Cartesian coordinate, such as, a flow around a square cylinder (Kimura and Hosoda, 1999), a flow around a surface-mounted cube (Kimura and Hosoda, 2000) and a compound open channel flow (Kimura et al, 2001). The constitutive equations of the model are described as

$$-\overline{v^{\prime\prime} v^{\prime j}} = D_t S^{ij} - \frac{2}{3} k \delta_s^i g^{sj} - \frac{k}{\varepsilon} D_t \left[\alpha_1 Q_1 + \alpha_2 Q_2 + \alpha_3 Q_3 \right] \tag{7}$$

$$D_t = C_\mu \frac{k^2}{\varepsilon} \tag{8}$$

$$Q_1 = S^{i\alpha} g_{\alpha\beta} \Omega^{\beta j} + S^{j\beta} g_{\beta\alpha} \Omega^{\alpha i} \tag{9}$$

$$Q_2 = S^{i\alpha} g_{\alpha\beta} S^{\beta j} - \frac{1}{3} S^{k\alpha} g_{\alpha m} S^{m\beta} g_{\beta k} \delta_l^i g^{lj} \tag{10}$$

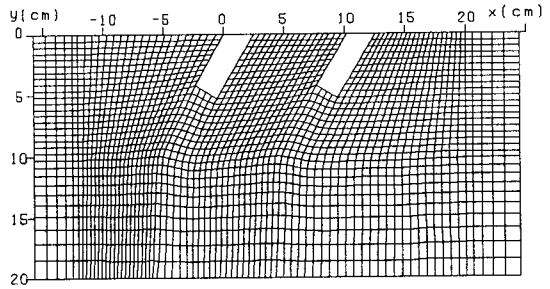

Figure 2: Numerical grid around the spur-dikes (Run 1).

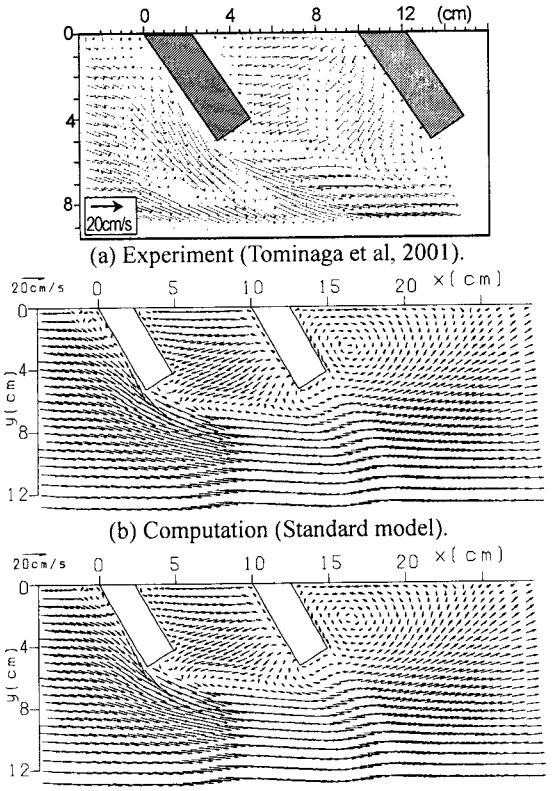

Figure 3: Time-mean horizontal flow patterns in Run 2 (z=5mm).

$$Q_3 = \Omega^{i\alpha} g_{\alpha\beta} \Omega^{\beta j} - \frac{1}{3} \Omega^{k\alpha} g_{\alpha m} \Omega^{m\beta} g_{\beta k} \delta_l^i g^{lj} \tag{11}$$

$$S^{ij} = g^{j\alpha} \nabla_\alpha V^i + g^{i\alpha} \nabla_\alpha V^j \tag{12}$$

$$\Omega^{ij} = g^{j\alpha} \nabla_\alpha V^i - g^{i\alpha} \nabla_\alpha V^j \tag{13}$$

The model coefficients are given as functions of the strain parameter S and the rotation parameter Ω as follows.

$$\alpha_1 = -0.1325 f_M, \quad \alpha_2 = 0.0675 f_M, \quad \alpha_3 = -0.0675 f_M \tag{14}$$

$$f_M = \left[1 + 0.02 M^2 \right]^{-1}, \quad M = \max[S, \Omega] \tag{15}$$

$$C_\mu = \min\left[0.09, 0.3/(1 + 0.09 M^2) \right] \tag{16}$$

$$S = \frac{k}{\varepsilon} \sqrt{\frac{1}{2} S^{i\alpha} g_{\alpha j} S^{j\beta} g_{\beta i}}, \quad \Omega = \frac{k}{\varepsilon} \sqrt{\frac{1}{2} \Omega^{i\alpha} g_{\alpha j} \Omega^{j\beta} g_{\beta i}} \tag{17}$$

Equations (14) and (15) were adjusted through the consideration of the distribution of turbulent intensities in a simple shear flow (Kimura and Hosoda, 2000). Equation (16) was tuned to satisfy the realizability in 2D and 3D

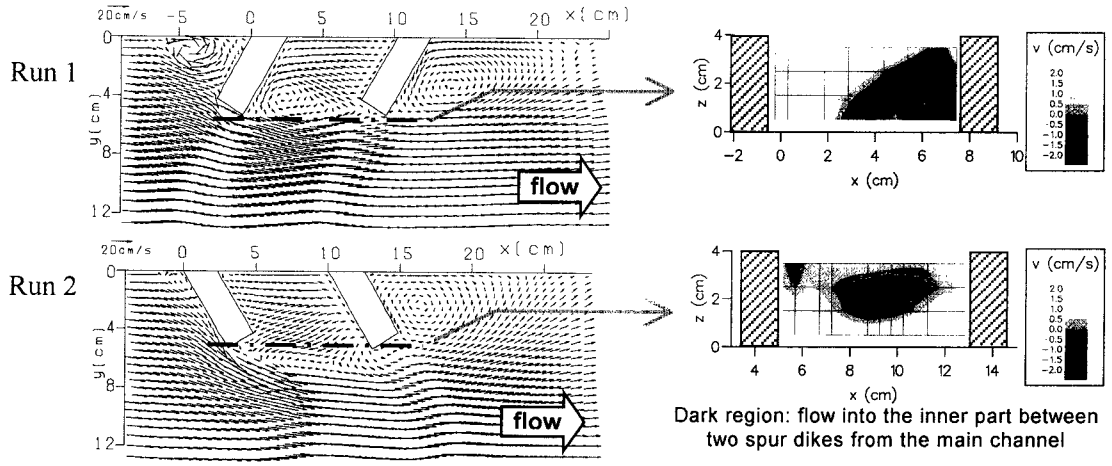

(a) Velocity vectors near the bed (z=5mm) (b) Flow distribution in a vertical section at y=45mm.

Figure 4: Time-mean flow field in the numerical results with the non-linear k-ε model.

flows (Hosoda et al, 2001).

Outline of Numerical Method

The differential equations governing the mean-velocities and the turbulence field are solved with the finite volume method on full-staggered grid system. The metric tensor and Cristoffel symbol are defined only at grid points to save computer memory and the values at other positions are interpolated at each computational step.

QUICK scheme is applied to the convection terms and the central differencing is used for the diffusion terms in the momentum equations. The hybrid central upwind scheme is applied to the k and ε equations. Adams-Bashforth scheme with second-order accuracy in time is used for time integration in each equation. The basic equations are discretized as fully explicit forms and are solved successively along the time axis step by step. The pressure field is solved using iterative procedure at each time step (Hirt et al, 1975).

Boundary and Initial Conditions

The wall function approach is applied as the wall boundary conditions for k and ε. The wall friction is evaluated by the log-law. At the downstream end, the longitudinal gradients of all variables are assumed to be zero. At the boundary inlet, the level of k is chosen to be $(0.02U_0)^2$ (U_0 = averaged velocity). The value of ε at the inlet is determined from the value of k at the inlet and Equation (8) by specifying the ratio $D_t/\nu = 10$ (Bosche and Rodi, 1998).

The free surface elevation is solved by the simple relation in Equation (18) since the contravariant components of the velocity vector are used in the basic equations.

$$\Delta h = \sqrt{g_{33}} V^3 \Delta t \tag{18}$$

where Δt = time increment and Δh = surface elevation during Δt. To consider the rapid attenuation of turbulent intensities in the depth-wise direction near the free surface, the eddy viscosity is multiplied by the following dumping function (Hosoda, 1990).

$$f_s = 1 - \exp\left(-B \frac{(h-y)\varepsilon_s}{k_s^{3/2}} \right), \quad (B = 10) \tag{19}$$

where sub-s indicates the value at the surface layer. The turbulent dissipation rate at the surface layer is evaluated by the following formula proposed by Sugiyama et al (1995) to calculate the secondary currents of 2nd kind.

$$\varepsilon_s = \frac{C_{\mu 0}^{3/4} k_s^{3/2}}{0.4 \Delta y_s}, \quad (C_{\mu 0} = 0.09) \tag{20}$$

At the beginning of the calculation, U (= velocity in longitudinal direction) = U_0 (=averaged velocity), V (= velocity in transverse direction) = 0, $k = k_{in}$ and $\varepsilon = \varepsilon_{in}$ (k_{in} and ε_{in} are the values of k and ε at the inlet boundary) are specified over the whole computational domain.

Hydraulic Conditions and Computational Domain

The computations are performed under the same conditions with the laboratory tests by Tominaga et al (2001). The hydraulic conditions in the computations are listed in Table 1. Two submerged spur dikes are placed at the left side of the flume. Two cases with different inclination angles, namely, upstream inclined (Run 1) and downstream inclined (Run 2) spur dikes are considered. The inclination angles with respect to the main flow direction in Runs 1 and 2 are 120° and 60°, respectively.

Numerical grids in the x-y plane at the vicinity of spur dikes in Runs 1 and 2 are shown together with the coordinate system in Figures 2 and 3, respectively. These grids are generated with the aid of the grid generator "Rubbnet" developed by Chiba and Takemoto (1999). The grid in vertical direction in each case is made by dividing the depth into 8 equal lengths. The grid over the roof of the spur dikes is moved in vertical direction according with the surface elevation calculated by Equation (18) at each time step. The number of grid points in each case becomes 104 (x-direction) × 30 (y-direction) × 8 (z-direction).

RESULTS AND DISCUSSIONS

Time-mean Flow Features

Since time-averaged flow features have been already reported in detail (Kimura et al, 2002b), we made some additional consideration focusing on the difference of turbulence models.

We first consider the flow near the bed, which is particularly important for sediment transport. Figure 3

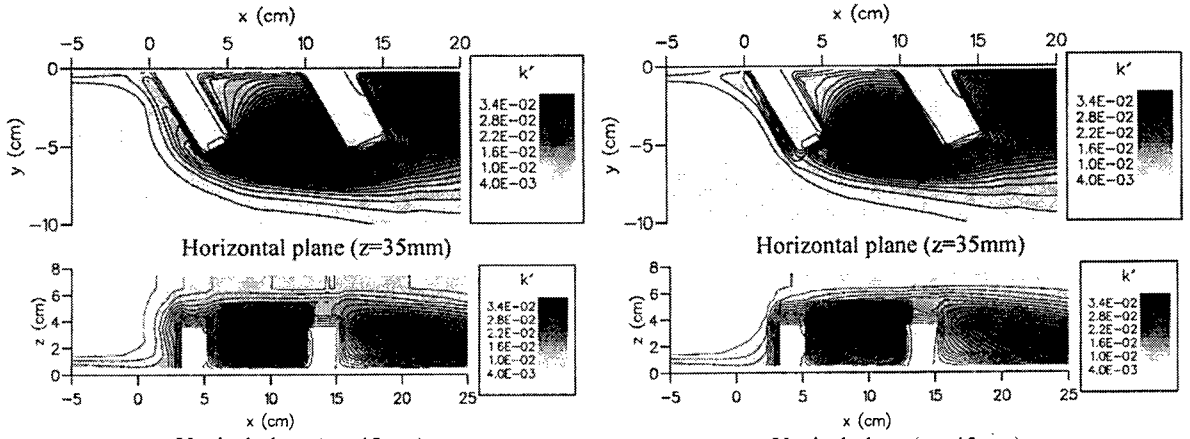

Figure 5: Comparison of dimensionless turbulence energy ($k'=k/U_0^2$), U_0 : bulk velocity).
(left: standard k-ε model, right: non-linear k-ε model)

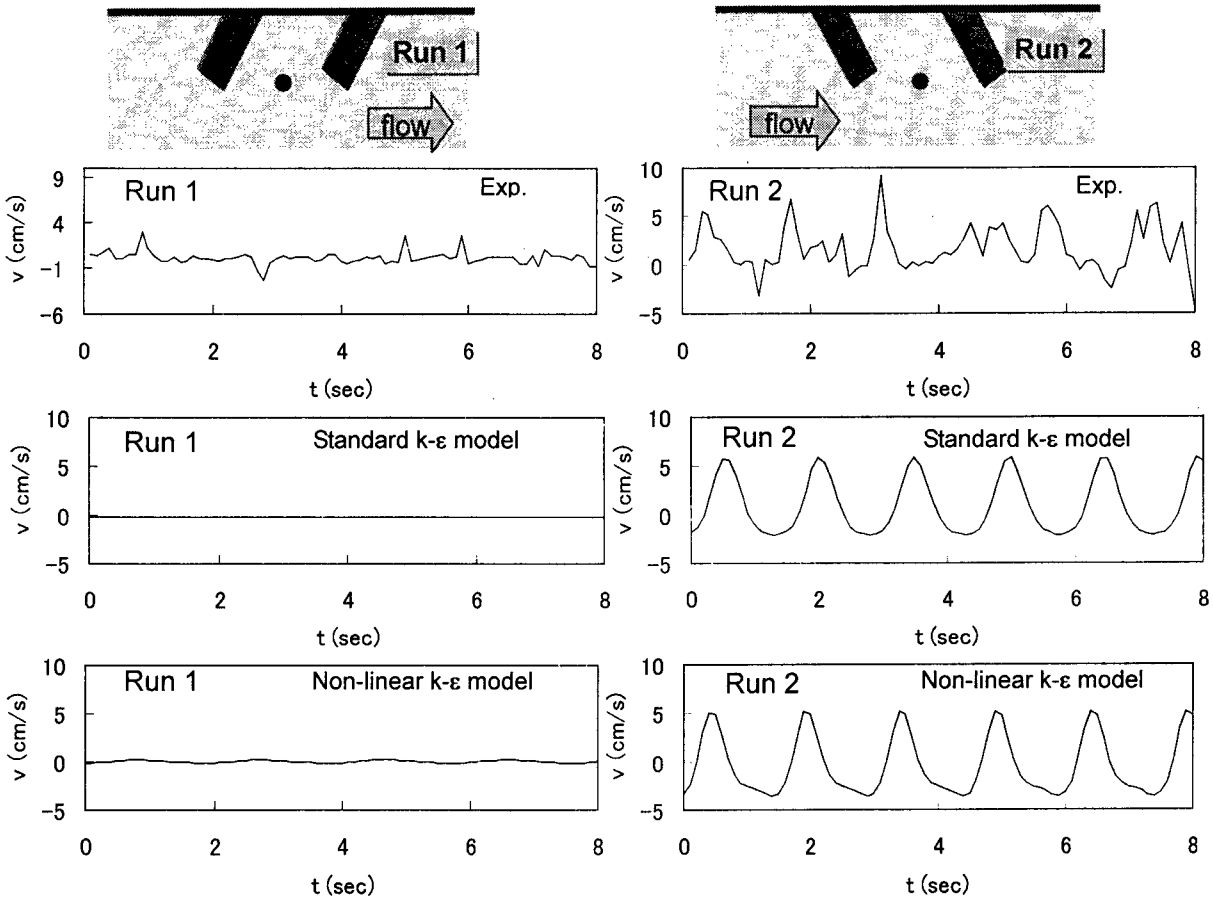

Figure 6: Temporal variation of velocity v at z=3.5cm at the interface (horizontal location are shown as ●).

shows the horizontal flow patterns in Run 2 at z = 5 mm by the laboratory test and different turbulence models. The flow patterns by two models are surprisingly similar. The reattachment length downstream of the second spur dike by the standard model is slightly longer than that by the non-linear model. The difference of the flow patterns in Run 1 by two models is also very small. The simulated flow patterns by both models are in good agreement with the experimental result. Figure 4 shows the plane velocity vectors near the bet and flow distributions in the vertical section at y = 45mm in the numerical results. This figure shows that, at the vicinity of bed, the flow from the inner part between two spur dikes toward the main channel is dominant around downstream inclined spur dikes, while the flow in the opposite direction is dominant around upstream inclined spur dikes.

Figure 5 shows the dimensionless turbulence energy k' ($=k/U_0^2$) in a horizontal plane at z = 35 mm and in a vertical plane at y = 45 mm. These figures show that the value of k' around the spur dikes by the non-linear model is smaller than that by the standard model. It has been pointed out that the standard model excessively products

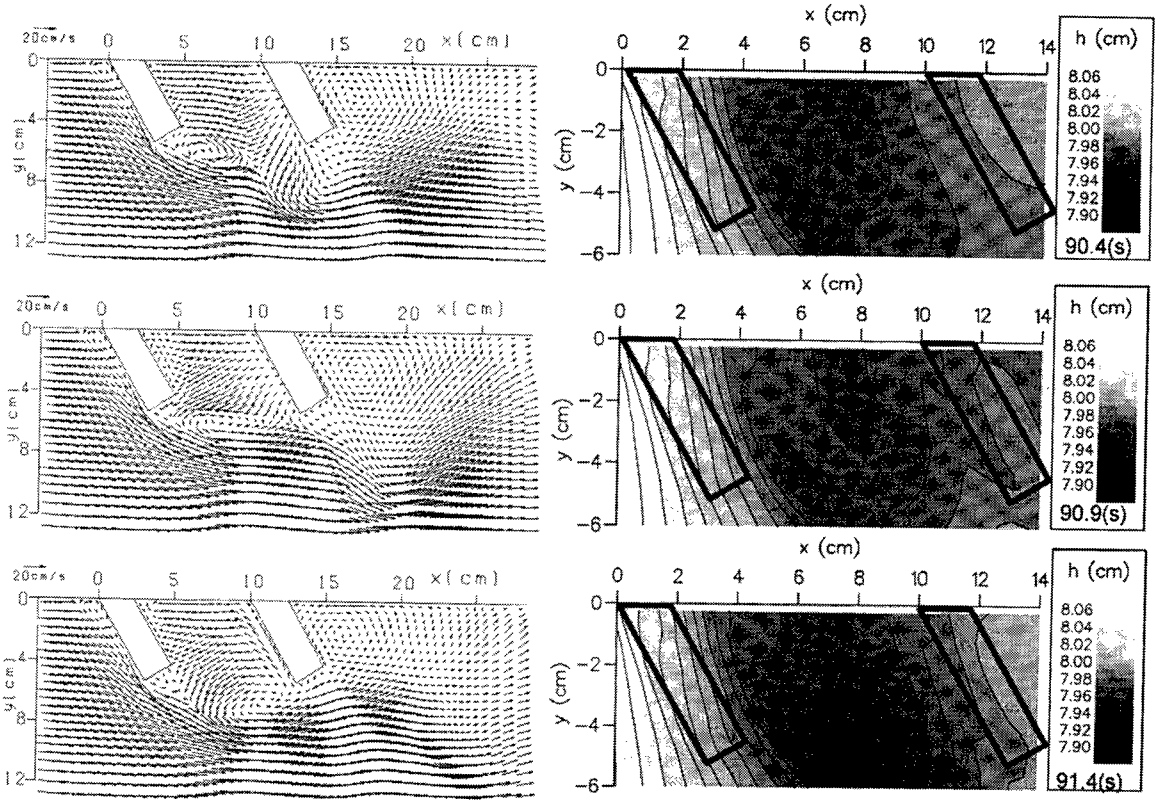

Figure 7: Time-dependent plane flow patterns by the non-linear model at z=5mm (left: velocity vector, right: depth).

the turbulence energy around the impinging region. In our previous works, the non-linear model can correct the shortcoming of the standard model to some extent. These results demonstrate again the advantage of the present non-linear model for the production of k around impinging region.

Unsteady Flow Characteristics

Effects of Inclination Angle on Unsteady Flow Features. Figure 6 shows the comparison of temporal velocity variations in y-direction between the experimental and numerical results. The locations of measured points are indicated in the diagrams as solid circles. In the experiment of Run 1, the flow is almost stable although slight fluctuation with small amplitude can be seen. The numerical results in Run 1 yield almost constant value regardless of the order of turbulence models. On the other hand, flow fluctuation can be seen in the experimental result in Run 2 and the period of the oscillation is not constant but variable from 0.5 to 2.0 sec. In the numerical results in Run 2, quite periodic oscillations are reproduced by both turbulence models. The periods in two models are same and are 1.3 sec. The amplitude of the oscillation by the non-linear model is a little larger than that by the standard model.

Figure 7 shows the velocity vectors at z = 5mm and the water surface level distributions in the numerical result at t = 90.4, 90.9, 91.4 sec. The vortex shedding from the tip of the first spur dike is numerically generated. The period of the vortex shedding is about 1.3 sec and is in agreement with the period of the velocity variation in Figure 6. The water level becomes local minimum around the center part of the vortex though the amplitude of the free surface oscillation is small.

Figure 8 shows the velocity vectors in the vertical plane at y = -50mm by the non-linear k-ε model. Intermittent upward flows can be seen at the downstream region of the first spur dike. It has been pointed out through the field observation that a boil is generated at the downstream region of spur dikes. The upward flow in the numerical result seems to be relevant to the boil.

The reason why the periodic motion is only generated around downstream inclined spur dikes is unclear. Note that the location of the separation at the first spur dike in two Runs are different, i.e., the separation occurs at the downstream / upstream corner of the tip of the first spur dike in Run 1 / Run 2. It is likely that the difference of separation points at the first spur dike is related with the magnitude of the unsteady oscillation.

Period of the Oscillation. The flow between two spur dikes is a typical case of impinging shear layers. The period of the fluid oscillation in the impinging shear layers is determined by the feedback effect. In the previous works of the impinging shear layers in various conditions, the Strouhal number of the first mode (the oscillation with the longest period) of the impinging shear layers satisfies the following equation (e.g. Rockewll et al, 1978).

$$St = \frac{fL}{U_0} \approx 0.4 \sim 0.6 \qquad (21)$$

where L: distance from the initial separation to the impinging point, U_0: bulk velocity and f: frequency of the fluid oscillation. Under the present conditions (L=10cm,

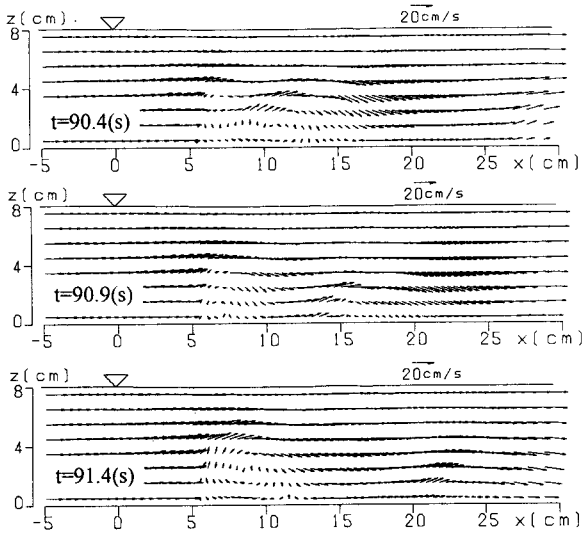

Figure 8: Time-dependent vertical flow features (non-linear model, y=-50.0mm)

U_0= 17.1cm/s, f=1/1.3 s^{-1}), the Strouhal number becomes 0.45 and is within the range of equation (21).

CONCLUDING REMARKS

3D turbulent flow features around inclined submerged spur dikes were numerically investigated with turbulence models focusing on the effects of the inclination angle. The standard linear k-ε model and 2nd order non-linear k-ε model were employed as turbulence models and numerical results were discussed through the comparison with the results of the laboratory tests by Tominaga et al (2002). The results in this study are summarized as follows.

1. The flow fields by two different turbulence models were quite similar though the turbulence energy around spur dikes by the non-liner model was smaller than that by the standard model.
2. The flow around upstream inclined spur dikes were almost steady in both experimental and numerical results, while, clear periodic oscillations with vortex shedding were generated around downstream inclined spur dikes.
3. The period of the fluid oscillation in the numerical results agrees with the first mode of impinging shear layer.

ACKNOWLEDGEMENT

The authors wish to express their sincere thanks to Prof. S. Chiba for the permission to use free his grid generator "Rubbnet". This study is partially supported by the Grant-in-Aid for Scientific Research, Ministry of Education, Science and Culture of Japan (No.14750433).

REFERENCES

Bosch, G. and Rodi, W, 1998, "Simulation of vortex shedding past a square cylinder with different turbulence models",. *Int. J. Numerical Methods in Fluids*, Vol.28, pp.601-616.

Chiba, S. and Takemoto, Y., 1999, "A Study of Numerical Flow Simulators of the Ise Bay, the Second Report –Development of a Computer Program for Generation of Two Dimensional Structural Grids, Making Use of Graphical User Interface–", *Yokkaichi Univ. J. Envir. and Info. Sci.*, Vol.2 (2), pp.103-126 (in Japanese).

Gatski, T.B. and Speziale, C.G., 1993, "On Explicit Algebraic Stress Models for Complex Turbulent Flows", *Journal of Fluid Mech*anics, Vol.254, pp. 59-78.

Hirt, C. W., Nichols, B. D. and Romero, N. C., 1975, "SOLA - a Numerical Solution Algorithm for Transient Fluid Flows", Los Alamos Scientific Report LA-5852.

Hosoda, T., 1990, Ph.D. Thesis, Kyoto University (in Japanese).

Hosoda, T., Kimura, I. and Onda, S., 2001, "Some Necessary Conditions for a Non-Linear k-ε Model in Classified Flow Patterns with a Singular Point", *Proceedings of 2nd International Symposium on Turbulence and Shear Flow Phenomena*, Stockholm, Sweden, Vol.3, pp. 155-160.

Hosoda, T., Sakurai, T., Kimura, I. and Muramoto, Y., 2000, "3-D Computations of Compound Open Channel Flows with Horizontal Vortices and Secondary Currents by Means of Non-linear k-ε Model. *J. Hydroscience and Hydraulic Eng.*, Vol.17, No.2, pp. 87-96.

Kawaguchi, H. and Fukuoka, S., 2000, "Study on Hydrodynamic Forces on Submersible Groins in Series", *Proceedings of Hydro Informatics*, Non-linear Analysis-2, Iowa City, IA, USA (CD-ROM).

Kimura, I. and Hosoda, T., 1999, "3-D Unsteady Flow Structures Around Rectangular Column in Open Channels by Means of Non-linear *k*-ε Model", *Proceedings of 1st International Symposium on Turbulence and Shear Flow Phenomena*, Santa Barbara, USA, pp. 1001-1006.

Kimura, I. and Hosoda, T., 2000, "Numerical Simulation of Flows Around a Surface-mounted Cube by Means of a Non-linear k-ε Model", *Proceedings of 9th. International Symposium on Flow Visualization*, Edinburgh, Scotland, Paper No.388 (CD-ROM).

Kimura, I., Hosoda, T. and Onda, S., 2002a, "Numerical Simulator on Full Staggered Boundary Fitted Coordinate System for the Analysis of 3D Turbulent Flows in Open Channels", *Yokkaichi University Journal of Environmental and Information Sciences*, Vol.4, No.1, pp. 145-170.

Kimura, I., Hosoda, T. and Onda, S., 2002b, "Prediction of 3D Flow Structures Around Skewed Spur Dikes by Means of a Non-linear k-ε Model", River Flow 2002 (eds. D.Bousmar and Y. Zech), Balkema, Vol.1, pp.65-73.

Rockwell, D. and Naudascher, E., 1978, "Review－Self-sustaining oscillations of flow past cavities", *Transaction of the ASME, Journal of Fluid Engineering*, Vol.100, pp.152-165.

Sugiyama, H., Akiyama, M. and Matsubara, T., 1995, "Numerical Simulation of Compound Open Channel Flow on Turbulence with a Reynolds Stress Model", *Journal of Hydraulic, Coastal and Environmental Eng*ineering, Vol. 515 / II -31, pp. 55-65 (in Japanese).

Takizawa, A., Koshizuka, S. and Kondo, S., 1992, "Generalization of Physical Component Boundary Fitted Co-ordinate (PCBFC) Method for the Analysis of Free-surface Flow. *International Journal for Numerical Methods in Fluids* Vol.15, pp. 1213-1237.

Tominaga, A., Ijima, K. and Nakao, Y., 2001, "PIV Analysis of Flow Structures Around Skewed Spur Dikes", *Annual Journal of Hydraulic Engineering, JSCE* Vol.42, pp. 379-384 (in Japanese).

Weitbrecht, V. and Jirka, H., 2001, "Flow Patterns in Dead Zones of Rivers and Their Effect on Exchange Processes", *Proceedings of 3rd International Symposium on Environmental Hydraulics*, Tempe, (CD-ROM).